

1 **Disintegration and Buttressing Effect of the Landfast**
2 **Sea Ice in the Larsen B Embayment, Antarctic**
3 **Peninsula**

4 **Yudong Sun¹, Bryan Riel^{1,2} and Brent Minchew¹**

5 ¹Department of Earth, Atmospheric, and Planetary Sciences, Massachusetts Institute of Technology,
6 Cambridge, MA, USA

7 ²School of Earth Sciences, Zhejiang University, Hangzhou, Zhejiang, China

8 **Key Points:**

- 9 • We present horizontal velocity and strain rate fields for Larsen B landfast sea ice
10 from 2014 to 2022
11 • Opening rifts may cause the landfast sea ice to break up
12 • Landfast sea ice provides negligible buttressing to the upstream glaciers

Corresponding author: Yudong Sun, yudong@mit.edu

Abstract

The speed-up of glaciers following ice shelf collapse can accelerate ice mass loss dramatically. Investigating the deformation of landfast sea ice enables studying its resistive (buttrressing) stresses and mechanisms driving ice collapse. Here, we apply offset tracking to Sentinel-1 A/B synthetic aperture radar (SAR) data to obtain a 2014-2022 time-series of horizontal velocity and strain rate fields of landfast ice filling the embayment formerly covered by the Larsen B Ice Shelf, Antarctic Peninsula until 2002. The landfast ice disintegrated in 2022, and we find that it was precipitated by a few large opening rifts. Upstream glaciers did not accelerate after the collapse, which implies little buttressing effect from landfast ice, a conclusion supported by the near-zero correlation between glacier velocity and landfast ice area. Our observations suggest that buttressing stresses are unlikely to be recovered by landfast sea ice over sub-decadal timescales following the collapse of an ice shelf.

Plain Language Summary

The Antarctic Ice Sheet is a potentially major contributor to sea-level rise due to glaciers' dynamic response to changing oceanic and atmospheric conditions. Its floating extensions, ice shelves, play a critical role in stabilizing the ice sheet by resisting the flow of glaciers that feed into them. However, ice shelves can collapse rapidly. In 2002, a Rhode Island-sized section of the Larsen B Ice Shelf disintegrated, causing adjacent glaciers to speed up. In 2011, landfast sea ice replaced the ice shelf in the Larsen B embayment, but it broke up in 2022. We use remote sensing data to investigate why the landfast ice collapsed and whether it resisted glacier flow as the ice shelf did. We show that opening rifts may be responsible for ice disintegration. We find no detectable buttressing effect from the landfast ice because glaciers did not speed up after removing landfast ice, and seasonal change of landfast ice extent did not affect the grounded glacier velocities. It may be because landfast ice is thinner and easier to deform than the ice shelf. Our observations suggest a possible precursor to ice collapse and highlight the limited role that landfast ice plays in slowing down ice mass loss.

1 Introduction

Acceleration of outlet glaciers in Antarctica can increase rates of sea-level rise. Because of their buttressing effect, ice shelves, which are the floating extensions of the ice sheets, play an essential role in regulating rates of mass loss in glaciers, and thus, sea-level rise (Mercer, 1978; Dupont & Alley, 2005; Bindschadler, 2006; DeConto & Pollard, 2016). More surface melt, basal melt, and iceberg calving can cause thinning, shrinking, and weakening of ice shelves due to the warming of the atmosphere and ocean (Shepherd et al., 2004; Pritchard et al., 2012; Depoorter et al., 2013; Lenaerts et al., 2017; Lai et al., 2020). The disintegration of some ice shelves, such as the Larsen A Ice Shelf in 1995 and Larsen B Ice Shelf in 2002 (both on the Antarctic Peninsula), led to the acceleration of some outlet glaciers by up to eight times the pre-collapse velocity (De Angelis & Skvarca, 2003; Rignot et al., 2004; T. A. Scambos et al., 2004).

From 2011 to 2022, the Larsen B embayment was covered with landfast sea ice, the quasi-stationary sea ice fastened to the coastline or islands (Armstrong (1972); Figure 1a). However, the landfast sea ice collapsed within several days in January 2022. Here, we aim to understand its disintegration mechanism and evaluate the buttressing of the landfast sea ice to determine if it could provide stabilizing effects in the case that ice shelves disintegrate.

We begin by studying the mechanisms for the catastrophic collapse of Larsen B landfast sea ice. Understanding the key mechanisms is important for monitoring the ice shelves, reducing sea-ice-related hazards, and understanding the couplings between the ice sheets,

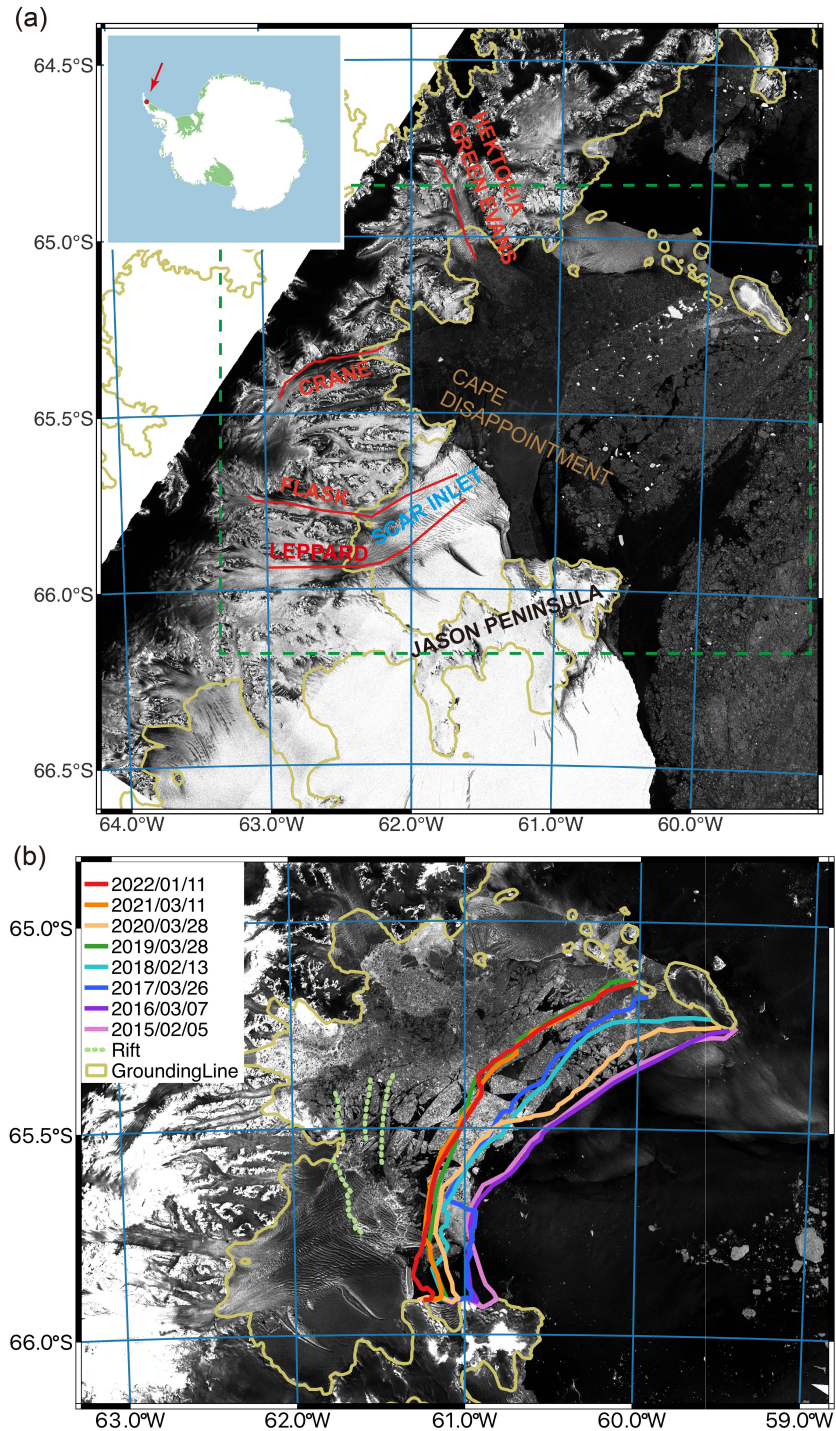


Figure 1. Sentinel-1 SAR amplitude image of the Larsen B area taken on September 30, 2020 (a). SAR image showing collapsed Larsen B landfast ice on January 23, 2022 (b). Yellow lines represent the grounding lines (Rignot et al., 2013; Mouginot et al., 2017). (a) Red lines show the profiles of four glaciers. Red arrow shows the location of our study area in the inserted subfigure. The dark green dash box indicates the approximate region for 1b. (b) Colored lines are the most retreated SLIEs for each year prior to collapse. Light green dashed lines denote the locations of pre-existing rifts.

62 sea ice, oceans, and the atmosphere. Hydrofracture by surface meltwater (Nye, 1957; Van der
 63 Veen, 1998), plate bending by buoyancy forces (Braun & Humbert, 2009; T. Scambos
 64 et al., 2009), sea ice loss, ocean swell (Massom et al., 2018), and crevasse-rift system (Glasser
 65 & Scambos, 2008; Rack & Rott, 2004) may have caused the disintegration of the Larsen
 66 A, B, and Wilkins Ice Shelves. One important observation is the widespread meltwater
 67 ponds on the Larsen Ice Shelf before disintegration (van den Broeke, 2005; Sergienko &
 68 MacAyeal, 2005), possibly related to foehn winds and atmospheric rivers (Cape et al.,
 69 2015; Wille et al., 2022). Several models, which consist of densely distributed melt-filled
 70 crevasses, have been proposed to explain the cascading collapse of ice shelves into small
 71 pieces in a short period (MacAyeal et al., 2003; Banwell et al., 2013; Robel & Banwell,
 72 2019). Meltwater ponding is observed every summer on the Larsen B landfast sea ice from
 73 Sentinel-1 SAR, Sentinel-2, and MODIS (Moderate Resolution Imaging Spectroradiome-
 74 ter) images. However, the mechanism for landfast sea ice disintegration may differ from
 75 the Larsen B Ice Shelf in 2002 due to different mechanical properties of the sea ice (Timco
 76 & Weeks, 2010).

77 Floating ice, restricted laterally by islands, peninsulas, or grounded icebergs, acts
 78 like the neck of an hourglass, slowing down the grounded glaciers flowing to the ocean.
 79 This buttressing effect can be quantitatively measured by the stress change at the ground-
 80 ing line after the hypothetical removal of the floating ice (Gudmundsson, 2013). It can
 81 also be evaluated by using ice-flow models with data assimilation, from which param-
 82 eters such as stress and viscosity can be estimated. Fürst et al. (2016) estimated the but-
 83 tressing potential of ice shelves by modeling the second principal horizontal stress (Doake
 84 et al., 1998), while Reese et al. (2018) studied it by calculating ice flux change due to
 85 the thinning of a given piece of the ice shelf. In terms of landfast ice, Greene et al. (2018)
 86 and Gomez-Fell et al. (2022) suggested that it can also buttress the ice shelves because
 87 the velocity of the ice shelves strongly correlates with the thickness or extent of land-
 88 fast ice. In this paper, we adopt this idea to study the buttressing effect of the landfast
 89 sea ice that occupied the Larsen B Embayment from 2011 to 2022.

90 2 Data and methods

91 We use repeated acquisitions from Sentinel-1 SAR (Supplementary Movie S1) to
 92 obtain the relative displacement of the ice surface using the offset tracking technique in
 93 the slant-range and azimuth directions, which are perpendicular and parallel to the flight
 94 direction, respectively (Strozzi et al., 2002; Joughin, 2002). Next, we use the predicted
 95 tide height in the model CATS2008 to remove vertical tidal motions from range displace-
 96 ments to isolate the horizontal displacements. Finally, we use a median filter to smooth
 97 the data in the spatial and temporal domains (see details in Supplementary Text S1 Sec-
 98 tion 1).

99 To show a cleaner map of velocity, we use two methods. In the first, we smooth the
 100 horizontal velocity maps (Supplementary Movie S2) with a second-order Savitzky–Golay
 101 filter (Savitzky & Golay, 1964) with a square window size of about 4 km. In the second
 102 method, we fit the velocity time-series in the temporal domain to remove the noise and
 103 make Movie S3 (horizontal velocity) using the time-series inversion package “iceutils.tseries”
 104 (Riel et al., 2014, 2021), which decomposes the signal into secular, seasonal, and tran-
 105 sient terms (see details in Supplementary Text S1 Section 3). Movie S2 has a higher spa-
 106 tial resolution, while Movie S3 is less noisy due to the smoothing inherent in the time-
 107 series method. Furthermore, we calculate the strain rate maps (Supplementary Movie
 108 S4 and S5) from the horizontal velocity maps (Movie S2). Movies S4 and S5 show hor-
 109 izontal dilation strain rate $\dot{\epsilon}_{dilate}$ (the trace of the horizontal strain rate tensor), max-
 110 imum shear strain rate $\dot{\epsilon}_{shear}$, strain rate along the flow direction $\dot{\epsilon}_{xx}$, and effective strain
 111 rate $\dot{\epsilon}_E$ (the second invariant of 3D strain rate tensor), respectively. These terms are de-
 112 fined in Supplementary Text S1 Section 4. To study the temporal change of landfast ice
 113 area, we use the cross-correlation method to find the stationary fast ice that moves less

114 than 100 m within 12 days (see details in Supplementary Text S1 Section 2), and delin-
 115 eate the seaward landfast ice edge (SLIE; colored lines in Figure 1b).

116 3 Results

117 3.1 Disintegration of landfast sea ice

118 A time-series of SAR images (collected from Sentinel-1 Path 38) shows the evolu-
 119 tion of ice shelves and sea ice (Movie S1). The Larsen B landfast sea ice collapsed into
 120 large pieces by January 23, 2022, later drifting counterclockwise on the ocean. It likely
 121 broke up between January 19 and 21, inferred from cloudy Moderate Resolution Imag-
 122 ing Spectroradiometer (MODIS) images from NASA’s Terra and Aqua satellites. Melange
 123 plumes appeared at the end of most glaciers, where ice fragment size is too small to see
 124 with SAR. A piece of the Scar Inlet Ice Shelf, comparable in size to the city of Philadel-
 125 phia, also broke off in this event. This disintegration is different from the 2002 event when
 126 only one giant melange plume was observed (Massom et al., 2018). This difference may
 127 be due to the sea ice pieces being too thin (Fraser et al., 2021) and too areally exten-
 128 sive to cause fragments to capsize (MacAyeal et al., 2003). After the disintegration, the
 129 Hektoria-Green-Evans Glacier retreated and lost about 200 square kilometers in late March
 130 (Movie S1).

131 The sea ice in Antarctica reached a new record low in 2022, probably due to a warmer
 132 ocean and strong winds (Raphael & Handcock, 2022). MODIS observed widespread melt-
 133 water ponds on the fast ice before disintegration. We investigate the locations of the SLIE
 134 every year when the landfast ice extent is the smallest (Figure 1b), which generally re-
 135 treats landward over the years except 2020. The landfast ice extent reached one of the
 136 lowest points just before the collapse in January 2022. The south end of SLIE retreated
 137 to the grounded ice (pinning point) near the Jason Peninsula, which also broke off later.
 138 Meanwhile, the Philadelphia-size iceberg calved along the opening rift on the Scar In-
 139 let Ice Shelf (green dashed line in Figure 1b). Most broken sea ice pieces near the Cape
 140 Disappointment are long and thin rectangles aligned in a similar direction as the rifts.
 141 Therefore, we suggest that the four opening rifts we identified in Section 3.3 may con-
 142 tribute to the collapse of the whole landfast ice.

143 3.2 Landfast sea ice buttressing

144 This collapsing event provides an opportunity to study the buttressing effect of the
 145 landfast sea ice. Some glaciers accelerated up to eightfold about nine months after the
 146 collapse of Larsen B Ice Shelf in 2002 (Rignot et al., 2004; T. A. Scambos et al., 2004;
 147 Wuite et al., 2015), but it remains unclear whether the sea ice provides enough buttress-
 148 ing stress to meaningfully slow down glaciers. Acceleration of upstream glaciers after the
 149 removal of landfast sea ice would show that landfast sea ice in the Larsen B embayment
 150 can generate sufficiently high resistive stresses to slow the flow of glaciers. However, the
 151 eight months of observations along profiles on four glaciers, which are similar locations
 152 as Rignot et al. (2004) (cf. their Figure 3) after the collapse, show no increase in speed
 153 (our Figure 2). The speed increase downstream of Hektoria-Green-Evans Glaciers in April
 154 (orange dots in Figure 2a) actually reflects the melange plume’s speed after the breakup
 155 (see details in Movie S1). Because our post-collapse observation time scale spans only
 156 eight months, we also analyze the horizontal velocity time-series before the collapse to
 157 study its relation with the landfast sea ice extent and buttressing effect.

158 Figure 3a and Movie S3 illustrate the evolution of velocity, the average of which
 159 is about 2 – 3 m/day in the Larsen B region and increases toward the seaward front.
 160 To extract the meaningful signals from the velocity time-series (dots in Figure 3d), we
 161 use the inversion method (Riel et al., 2014, 2021) to fit the curves (solid lines). Figure
 162 3d shows a small seasonal variation of velocity for the grounded glacier (red line; A in

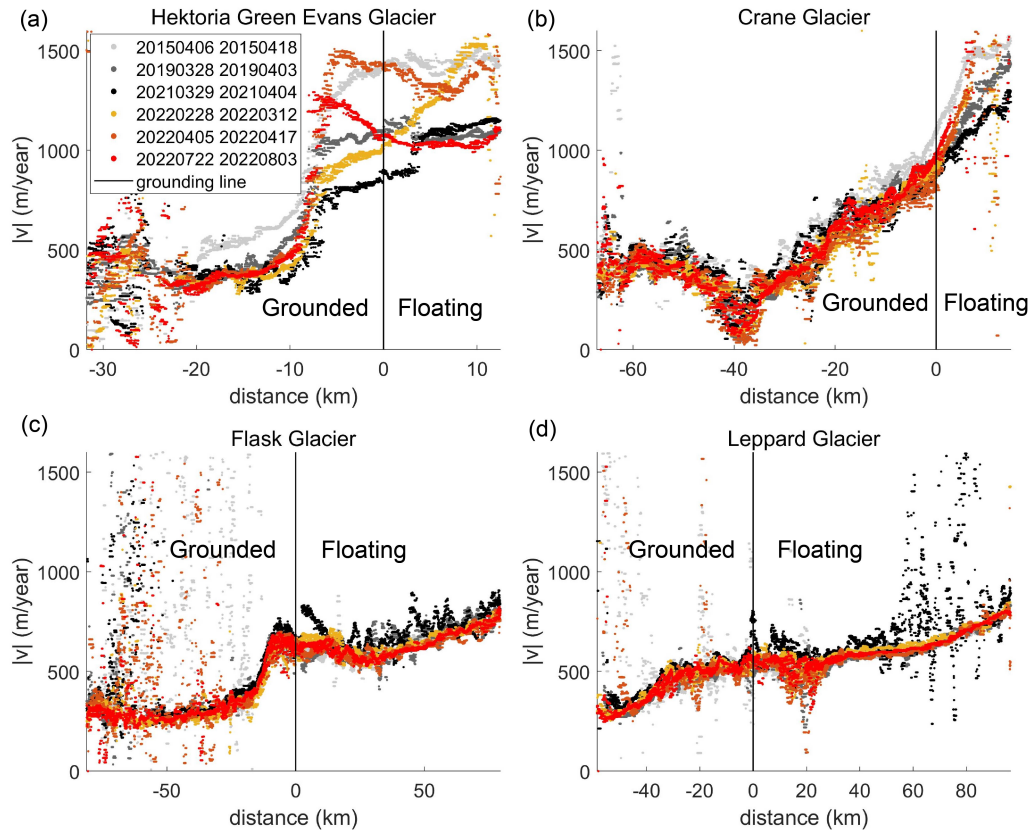


Figure 2. Speed along the profiles (red lines in Figure 1a) for four glaciers. The distance is relative to where the transect crosses the grounding line, with positive values being downstream on the floating ice. Different colors represent pairs for different times (format: `yyyymmdd`; before collapse: white, gray, and black; after collapse: yellow, orange, and red).

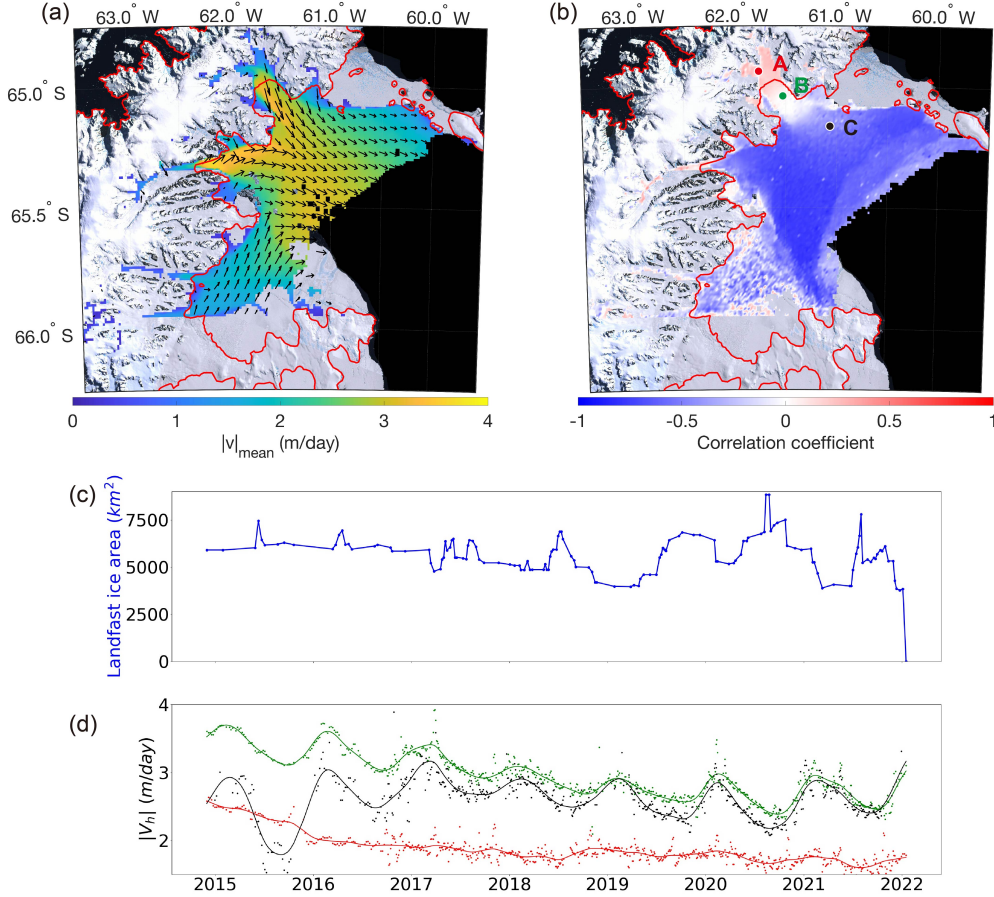


Figure 3. Horizontal velocity after time-series curve fitting and its relation with landfast ice extent. (a) The average horizontal velocity map of Larsen B embayment represented by both the colorbar and vectors. (b) The map of correlation coefficient between speed and landfast sea ice extent. (c) Evolution of the landfast sea ice extent. (d) Time-series of horizontal speed (dots) and fitting lines at 3 locations denoted by dots (Figure 3b). The red lines show the grounding lines and the background map is the Landsat Image Mosaic of Antarctica (Bindschadler et al., 2008) (Figure 3a and b).

163
164

Figure 3b). In contrast, the seasonal variation gets larger downstream on the landfast sea ice (green and black lines; B and C in Figure 3b).

165
166
167
168
169
170
171
172
173
174
175
176

To evaluate the buttressing effect, we calculate the correlation coefficient between the landfast sea ice area (Figure 3c) and horizontal velocity. Sea ice adheres to the landfast sea ice, and its area gets larger in winter, while ice breaks away to reduce the areal extent in the summer (Movie S1). The landfast sea ice velocity shown in Figure 3d is higher in summer and lower in winter, so the correlation coefficient is generally negative. Buttressing stress comes from the confined margin of landfast ice with ice shelves, land, or islands (Gudmundsson, 2013; Schoof, 2007). Therefore, it should increase with the contact area between the ice and the solid Earth. We take the areal extent of the sea ice as a proxy for this contact area. Thus, if the velocity variation of the upstream glaciers negatively correlates with the extent of the landfast sea ice, the sea ice has a “tele-buttressing” effect, as discussed in Reese et al. (2018). We use a fitting curve from time-series inversion (Supplementary Text S1 Section 3) to do the correlation because the high-frequency

177 signals (with periods shorter than 10 days) are removed, giving a similar sampling rate
178 to the fast ice extent data.

179 We show correlation coefficients for every location where velocity data are avail-
180 able more than 50% of the time (Figure 3b). The correlation coefficient is negative on
181 the landfast sea ice, while it is near 0 on the glacier outlets and slightly below 0 on the
182 Scar Inlet Ice Shelf. The slight positive correlation on the Hecktoria-Green-Evans glacier
183 is due to the decreasing trend of velocity (Figure 3d). Our results suggest that the but-
184 tressing stress from the Larsen B landfast sea ice may not transmit to the upstream glaciers
185 due to a combination of thinner ice with different mechanical properties and materials
186 damaged from the previous long-lived ice shelves (Domack et al., 2005). This result agrees
187 with the observation of no speed-up after the removal. At this time, it is not clear how
188 to estimate the relative importance of buttressing of ice thickness and differing mechan-
189 ical properties between the sea ice pack and the Larsen B Ice Shelf, only to say that the
190 sea ice pack provided little buttressing relative to the ice shelf.

191 3.3 Rift and pressure ridge

192 The SLIE in Larsen B usually retreats from autumn to winter and advances from
193 spring to summer (blue line in Figure 3c). To study these processes and corresponding
194 rifts and pressure ridges, we take the gradient of the spatially-smoothed velocity field
195 to produce the strain maps (Movie S4 and S5; method discussed in Text S1 Section 4).
196 The strain-rate maps ($\dot{\epsilon}_{dilate}$ in Movie S4) show high compressional strain rates (blue)
197 at the boundary when the drift ice sticks to the landfast ice. This signal indicates the
198 formation of the pressure ridge (Feltham, 2008), which originates from the collision of
199 two pieces of ice driven by wind or ocean currents. We also observe rifts with a high ex-
200 tensional strain rate (red) several days before a piece of ice breaks away from the land-
201 fast ice in Movie S4. Therefore, we can consider this phenomenon as a precursor to the
202 ice-calving event.

203 We show two cases with rifts and pressure ridges inside the landfast sea ice in Fig-
204 ure 4. First, pressure ridges (in blue) showed up at the downstream landfast sea ice of
205 the Hektoria, Crane Glaciers, and Scar Inlet Ice Shelf from June to September in 2015
206 (Figure 4a). This event happened when the upstream glaciers accelerated (red dots in
207 Figure 3d), so the downstream landfast ice was in compression. If the sea ice is mechan-
208 ically strong and coherent, there will be a widespread slightly-compressed zone. There-
209 fore, the localized compressional arches indicate that sea ice deforms plastically, and stress
210 becomes independent of strain when it exceeds a certain yield criterion. We suggest this
211 is because sea ice is porous and has low cohesion (Timco & Weeks, 2010; Feltham, 2008;
212 Hibler, 1979).

213 Second, Figure 4d shows three rifts near Cape Disappointment and one on the Scar
214 Inlet Ice shelf, which emerged during the observation period and probably caused the
215 collapse of the whole landfast sea ice pack (also marked as green dashed lines in Figure
216 1b). Movie S4 shows that the dilatation strain rate in these rifts is positive continuously,
217 which means they opened plastically after they fractured. The western rift on the land-
218 fast sea ice connects with the rift on the ice shelf, which suggests the landfast ice me-
219 chanically couples with the ice shelf to some extent. Three opening rifts fractured be-
220 cause the northeast-moving Scar Inlet Ice Shelf protruded into the landfast ice, and it
221 pulled apart the landfast sea ice on the northern side (see velocity directions in Figure
222 3a). The rift on the front of the Scar Inlet Ice Shelf ruptured because the east-moving
223 landfast ice sheared the indented piece, and the ice shelf was also in an extensional en-
224 vironment. Therefore, these observations suggest that the relative motions of the land-
225 fast ice and ice shelf are mainly responsible for the formation of the rifts.

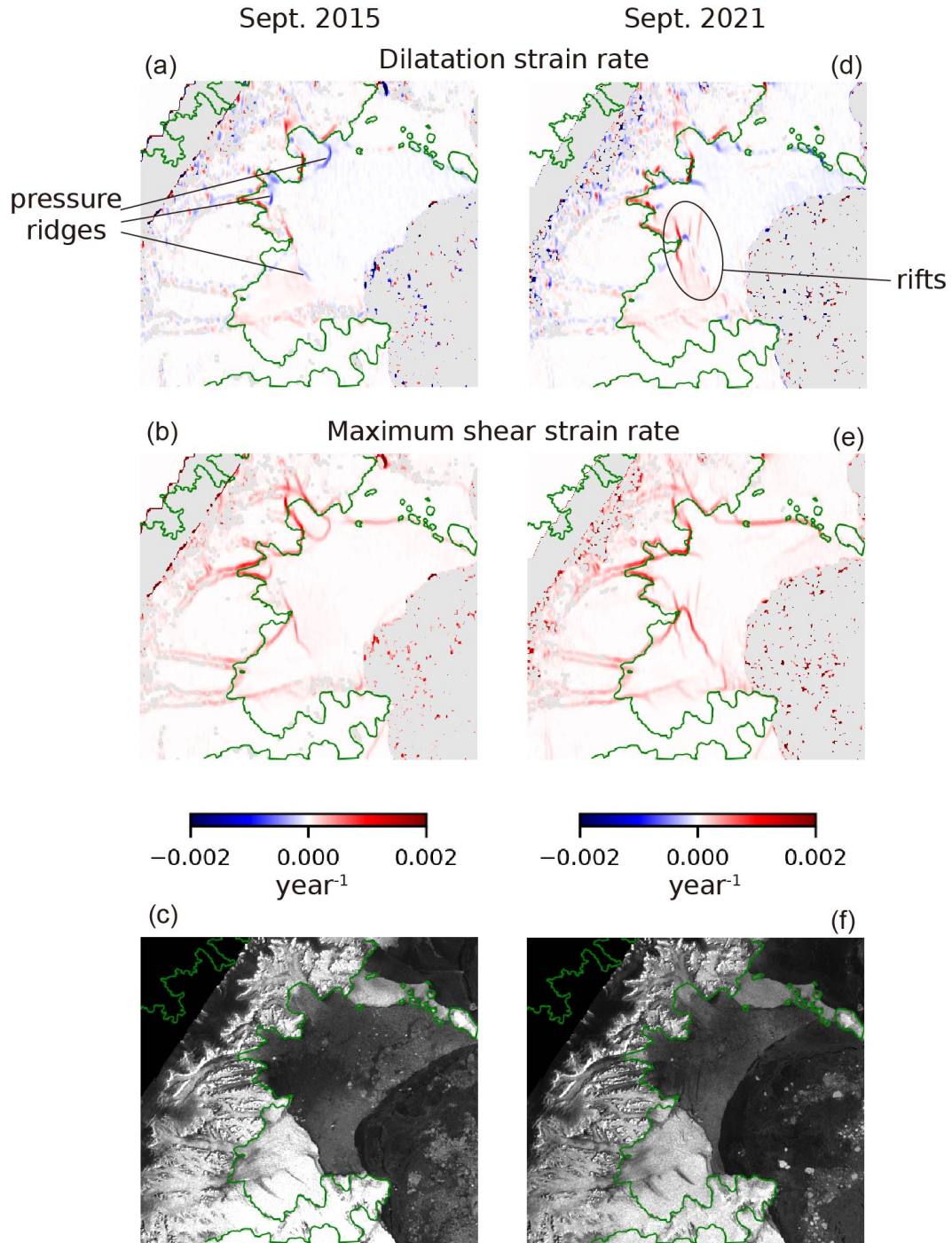


Figure 4. The dialation strain rate $\dot{\epsilon}_{dilate}$, shear strain rate $\dot{\epsilon}_{shear}$ and SAR images in 2015 (a-c) and 2021 (b-f). The strain rate maps represent the deformation between Sept. 9 and Sept. 21, 2015 (a, b), and between Sept. 13 and Sept. 19, 2021 (d, e), respectively. The SAR intensity images are taken on Sept. 21, 2015, and Sept. 19, 2021, respectively. Red represents extension while blue represents compression for the $\dot{\epsilon}_{dilate}$ maps (a, d). Green lines indicate the grounding lines.

4 Discussion and conclusion

The horizontal velocity fields derived from SAR data provide multiple lines of evidence showing that the sea ice pack that filled the Larsen B embayment from 2014 to 2022 provided little buttressing to the grounded glaciers. We find no glacier acceleration after fast ice disintegration and no correlation between glacier velocity and landfast sea ice extent. This is because fast ice is thinner and weaker than the ice shelf that filled the embayment prior to 2002. These characteristics cause landfast sea ice to readily develop large-scale damage features, including the pressure ridges and opening rifts we observe, which reduce the sea ice pack's ability to provide buttressing stresses.

Our argument of negligible buttressing from the sea ice pack is supported by the absence of observable glacier acceleration in the first eight months following the collapse of the ice pack. This result differs from observations following the collapse of the Larsen B Ice Shelf that showed a significant velocity increase on the Crane and Hektoria-Green-Evans Glaciers one year after the collapse (Rignot et al., 2004). We attribute this difference to the fact that the Larsen B Ice Shelf was much thicker and likely more competent at the time of its collapse than the sea ice pack, which allowed the ice shelf to support higher buttressing stresses.

The second piece of evidence is that we find no negative correlation between fast ice extent and velocity on the glaciers. Specifically, the seasonal fluctuation of horizontal velocity is large on the fast ice but is negligibly small on the grounded glaciers and the Scar Inlet Ice Shelf. In contrast, Greene et al. (2018) and Gomez-Fell et al. (2022) found a good correlation between sea ice extent and ice shelf velocity in other areas, probably because their study areas have different geographical locations relative to the ocean and land. For example, the Parker Ice Tongue studied in Gomez-Fell et al. (2022) protrudes into the surrounding sea ice and is thus more sensitive to changes in buttressing at the calving front. Furthermore, the difference between those studies and ours is due to the fact that we also focus on grounded glaciers, which have additional basal drag to resist changes in flow.

We observe the formation of four opening rifts from the strain rate maps (Figure 4d), which may contribute to the disintegration of the whole landfast sea ice. They are much longer than that found on the previous Larsen B Ice Shelf (Glasser & Scambos, 2008), which can undermine the structural integrity of the sea ice pack, further leading to its collapse. We also observe that the fast ice collapsed differently from the ice shelf collapse in 2002. A large melange plume was observed after the collapse in 2002, but the landfast sea ice broke up into large pieces, which implies that sea ice is too thin to capsize and cannot break up in a cascade.

Taken together, the decade-long observations of the Larsen B embayment show that the landfast sea ice that occupied the same area as the Larsen B Ice Shelf did not provide the same buttressing stress as the previous ice shelf, suggesting that if more ice shelves collapse due to climate change, the upstream glaciers will likely accelerate regardless of sea ice conditions. In other words, this finding suggests that ice shelf buttressing is not renewable over sub-decadal timescales. Our observations also elucidate ice-ocean-atmosphere interaction and help to monitor sea-ice-related hazards. For instance, the shrinking landfast sea ice and the large seasonal variation of its horizontal velocity we observe have the potential to illuminate how the ocean and climate influence ice evolution. In addition, the transient signals of high strain rates can be used as precursors for calving events or massive ice collapses.

Open Research Section

We use Copernicus Sentinel-1 synthetic SAR data from 2014 to 2022, retrieved from ASF DAAC and processed by ESA (<https://search.asf.alaska.edu/>). We use the

276 InSAR Scientific Computing Environment ISCE (Rosen et al., 2012) to perform the pixel
277 offset tracking (<https://github.com/isce-framework>). The tide model CATS2008 (Padman
278 et al., 2002, 2008) for tide correction is available at [https://www.esr.org/research/
279 polar-tide-models/list-of-polar-tide-models/cats2008/](https://www.esr.org/research/polar-tide-models/list-of-polar-tide-models/cats2008/). The software “iceutils”
280 (Riel et al., 2014, 2021) for filtering and strain rate calculation is available at [https://
281 github.com/bryanvriel/iceutils](https://github.com/bryanvriel/iceutils). We use the software “hyp3.timeseries” ([https://
282 github.com/jlinick/hyp3.timeseries](https://github.com/jlinick/hyp3.timeseries)) to make Supplementary Movie S1. We use the
283 QGIS (<https://qgis.org/en/site/forusers/download.html>) and Qantarctica soft-
284 ware (<https://www.npolar.no/quantarctica/>) to plot Figure 1. Our final data prod-
285 ucts, including velocity and strain rate fields used in Movie S2-S5, are archived in Zen-
286 odo (<https://doi.org/10.5281/zenodo.7818543>).

287 **Acknowledgments**

288 The authors thank Camilla Cattania, Justin Linick, Colin Meyer, Enrico Milanese,
289 Joanna Millstein, Meghana Ranganathan, and Sarah Wells-Moran for helpful discussions.
290 Y.S. received fundings from MIT EAPS Robert R Shrock Fellowship, Sven Treitel (1953)
291 Fellowship, and MIT Mathworks Fellowship. B.M. and B.R. received funding from NSFGEO-
292 NERC grant 1853918, the John W. Jarve (1978) Seed Fund for Science Innovation, and
293 the Earl A Killian III (1978) and Waidy Lee Fund.

References

- 294
- 295 Armstrong, T. (1972). World meteorological organization. wmo sea-ice nomen-
 296 clature. terminology, codes and illustrated glossary. edition 1970. geneva,
 297 secretariat of the world meteorological organization, 1970.[ix], 147 p.[including
 298 175 photos]+ corrigenda slip.(wmo/omm/bmo, no. 259, tp. 145.). *Journal of*
 299 *Glaciology*, 11(61), 148–149.
- 300 Banwell, A. F., MacAyeal, D. R., & Sergienko, O. V. (2013). Breakup of the larsen b
 301 ice shelf triggered by chain reaction drainage of supraglacial lakes. *Geophysical*
 302 *Research Letters*, 40(22), 5872–5876.
- 303 Bindschadler, R. (2006). Hitting the ice sheets where it hurts. *Science*, 311(5768),
 304 1720–1721.
- 305 Bindschadler, R., Vornberger, P., Fleming, A., Fox, A., Mullins, J., Binnie, D., ...
 306 Gorodetzky, D. (2008). The landsat image mosaic of antarctica. *Remote*
 307 *Sensing of Environment*, 112(12), 4214–4226.
- 308 Braun, M., & Humbert, A. (2009). Recent retreat of wilkins ice shelf reveals new in-
 309 sights in ice shelf breakup mechanisms. *IEEE Geoscience and Remote Sensing*
 310 *Letters*, 6(2), 263–267.
- 311 Cape, M., Vernet, M., Skvarca, P., Marinsek, S., Scambos, T., & Domack, E. (2015).
 312 Foehn winds link climate-driven warming to ice shelf evolution in antarctica.
 313 *Journal of Geophysical Research: Atmospheres*, 120(21), 11–037.
- 314 De Angelis, H., & Skvarca, P. (2003). Glacier surge after ice shelf collapse. *Science*,
 315 299(5612), 1560–1562.
- 316 DeConto, R. M., & Pollard, D. (2016). Contribution of antarctica to past and future
 317 sea-level rise. *Nature*, 531(7596), 591–597.
- 318 Depoorter, M. A., Bamber, J. L., Griggs, J. A., Lenaerts, J. T., Ligtenberg, S. R.,
 319 van den Broeke, M. R., & Moholdt, G. (2013). Calving fluxes and basal melt
 320 rates of antarctic ice shelves. *Nature*, 502(7469), 89–92.
- 321 Doake, C., Corr, H., Rott, H., Skvarca, P., & Young, N. (1998). Breakup and
 322 conditions for stability of the northern larsen ice shelf, antarctica. *Nature*,
 323 391(6669), 778–780.
- 324 Domack, E., Duran, D., Leventer, A., Ishman, S., Doane, S., McCallum, S., ...
 325 Prentice, M. (2005). Stability of the larsen b ice shelf on the antarctic penin-
 326 sula during the holocene epoch. *Nature*, 436(7051), 681–685.
- 327 Dupont, T., & Alley, R. (2005). Assessment of the importance of ice-shelf buttress-
 328 ing to ice-sheet flow. *Geophysical Research Letters*, 32(4).
- 329 Feltham, D. L. (2008). Sea ice rheology. *Annu. Rev. Fluid Mech.*, 40, 91–112.
- 330 Fraser, A. D., Massom, R. A., Handcock, M. S., Reid, P., Ohshima, K. I., Raphael,
 331 M. N., ... Porter-Smith, R. (2021). Eighteen-year record of circum-antarctic
 332 landfast-sea-ice distribution allows detailed baseline characterisation and re-
 333 veals trends and variability. *The Cryosphere*, 15(11), 5061–5077.
- 334 Fürst, J. J., Durand, G., Gillet-Chaulet, F., Tavard, L., Rankl, M., Braun, M., &
 335 Gagliardini, O. (2016). The safety band of antarctic ice shelves. *Nature*
 336 *Climate Change*, 6(5), 479–482.
- 337 Glasser, N., & Scambos, T. A. (2008). A structural glaciological analysis of the 2002
 338 larsen b ice-shelf collapse. *Journal of Glaciology*, 54(184), 3–16.
- 339 Gomez-Fell, R., Rack, W., Purdie, H., & Marsh, O. (2022). Parker ice tongue col-
 340 lapse, antarctica, triggered by loss of stabilizing land-fast sea ice. *Geophysical*
 341 *Research Letters*, 49(1), e2021GL096156.
- 342 Greene, C. A., Young, D. A., Gwyther, D. E., Galton-Fenzi, B. K., & Blankenship,
 343 D. D. (2018). Seasonal dynamics of totten ice shelf controlled by sea ice
 344 buttressing. *The Cryosphere*, 12(9), 2869–2882.
- 345 Gudmundsson, G. (2013). Ice-shelf buttressing and the stability of marine ice sheets.
 346 *The Cryosphere*, 7(2), 647–655.
- 347 Hibler, W. D. (1979). A dynamic thermodynamic sea ice model. *Journal of physical*
 348 *oceanography*, 9(4), 815–846.

- 349 Joughin, I. (2002). Ice-sheet velocity mapping: a combined interferometric and
 350 speckle-tracking approach. *Annals of Glaciology*, *34*, 195–201.
- 351 Lai, C.-Y., Kingslake, J., Wearing, M. G., Chen, P.-H. C., Gentine, P., Li, H.,
 352 ... van Wessem, J. M. (2020). Vulnerability of antarctica’s ice shelves to
 353 meltwater-driven fracture. *Nature*, *584*(7822), 574–578.
- 354 Lenaerts, J., Lhermitte, S., Drews, R., Ligtenberg, S., Berger, S., Helm, V., ... oth-
 355 ers (2017). Meltwater produced by wind–albedo interaction stored in an east
 356 antarctic ice shelf. *Nature climate change*, *7*(1), 58–62.
- 357 MacAyeal, D. R., Scambos, T. A., Hulbe, C. L., & Fahnestock, M. A. (2003). Cata-
 358 strophic ice-shelf break-up by an ice-shelf-fragment-capsize mechanism. *Journal*
 359 *of Glaciology*, *49*(164), 22–36.
- 360 Massom, R. A., Scambos, T. A., Bennetts, L. G., Reid, P., Squire, V. A., & Stam-
 361 merjohn, S. E. (2018). Antarctic ice shelf disintegration triggered by sea ice
 362 loss and ocean swell. *Nature*, *558*(7710), 383–389.
- 363 Mercer, J. H. (1978). West antarctic ice sheet and co2 greenhouse effect: a threat of
 364 disaster. *Nature*, *271*(5643), 321–325.
- 365 Mouginot, J., Scheuchl, B., & Rignot, E. (2017). Measures antarctic boundaries
 366 for ipy 2007–2009 from satellite radar, version 2. *National Snow and Ice Data*
 367 *Center*, *10*.
- 368 Nye, J. F. (1957). The distribution of stress and velocity in glaciers and ice-sheets.
 369 *Proceedings of the Royal Society of London. Series A. Mathematical and Physi-*
 370 *cal Sciences*, *239*(1216), 113–133.
- 371 Padman, L., Erofeeva, S. Y., & Fricker, H. A. (2008). Improving antarctic tide
 372 models by assimilation of icesat laser altimetry over ice shelves. *Geophysical*
 373 *Research Letters*, *35*(22).
- 374 Padman, L., Fricker, H. A., Coleman, R., Howard, S., & Erofeeva, L. (2002). A
 375 new tide model for the antarctic ice shelves and seas. *Annals of Glaciology*, *34*,
 376 247–254.
- 377 Pritchard, H., Ligtenberg, S. R., Fricker, H. A., Vaughan, D. G., van den Broeke,
 378 M. R., & Padman, L. (2012). Antarctic ice-sheet loss driven by basal melting
 379 of ice shelves. *Nature*, *484*(7395), 502–505.
- 380 Rack, W., & Rott, H. (2004). Pattern of retreat and disintegration of the larsen b
 381 ice shelf, antarctic peninsula. *Annals of glaciology*, *39*, 505–510.
- 382 Raphael, M. N., & Handcock, M. S. (2022). A new record minimum for antarctic sea
 383 ice. *Nature Reviews Earth & Environment*, 1–2.
- 384 Reese, R., Gudmundsson, G. H., Levermann, A., & Winkelmann, R. (2018). The far
 385 reach of ice-shelf thinning in antarctica. *Nature Climate Change*, *8*(1), 53–57.
- 386 Riel, B., Minchew, B., & Joughin, I. (2021). Observing traveling waves in glaciers
 387 with remote sensing: new flexible time series methods and application to ser-
 388 meq kujalleq (jakobshavn isbræ), greenland. *The Cryosphere*, *15*(1), 407–429.
- 389 Riel, B., Simons, M., Agram, P., & Zhan, Z. (2014). Detecting transient signals in
 390 geodetic time series using sparse estimation techniques. *Journal of Geophysical*
 391 *Research: Solid Earth*, *119*(6), 5140–5160.
- 392 Rignot, E., Casassa, G., Gogineni, P., Krabill, W., Rivera, A., & Thomas, R. (2004).
 393 Accelerated ice discharge from the antarctic peninsula following the collapse of
 394 larsen b ice shelf. *Geophysical research letters*, *31*(18).
- 395 Rignot, E., Jacobs, S., Mouginot, J., & Scheuchl, B. (2013). Ice-shelf melting around
 396 antarctica. *Science*, *341*(6143), 266–270.
- 397 Robel, A. A., & Banwell, A. F. (2019). A speed limit on ice shelf collapse through
 398 hydrofracture. *Geophysical Research Letters*, *46*(21), 12092–12100.
- 399 Rosen, P. A., Gurrola, E., Sacco, G. F., & Zebker, H. (2012). The insar scientific
 400 computing environment. In *Eusar 2012; 9th european conference on synthetic*
 401 *aperture radar* (pp. 730–733).
- 402 Savitzky, A., & Golay, M. J. (1964). Smoothing and differentiation of data by sim-
 403 plified least squares procedures. *Analytical chemistry*, *36*(8), 1627–1639.

- 404 Scambos, T., Fricker, H. A., Liu, C.-C., Bohlander, J., Fastook, J., Sargent, A.,
405 ... Wu, A.-M. (2009). Ice shelf disintegration by plate bending and hydro-
406 fracture: Satellite observations and model results of the 2008 wilkins ice shelf
407 break-ups. *Earth and Planetary Science Letters*, 280(1-4), 51–60.
- 408 Scambos, T. A., Bohlander, J., Shuman, C. A., & Skvarca, P. (2004). Glacier ac-
409 celeration and thinning after ice shelf collapse in the larsen b embayment,
410 antarctica. *Geophysical Research Letters*, 31(18).
- 411 Schoof, C. (2007). Ice sheet grounding line dynamics: Steady states, stability, and
412 hysteresis. *Journal of Geophysical Research: Earth Surface*, 112(F3).
- 413 Sergienko, O., & Macayeal, D. R. (2005). Surface melting on larsen ice shelf, antarc-
414 tica. *Annals of Glaciology*, 40, 215–218.
- 415 Shepherd, A., Wingham, D., & Rignot, E. (2004). Warm ocean is eroding west
416 antarctic ice sheet. *Geophysical Research Letters*, 31(23).
- 417 Strozzi, T., Luckman, A., Murray, T., Wegmuller, U., & Werner, C. L. (2002).
418 Glacier motion estimation using sar offset-tracking procedures. *IEEE Transac-
419 tions on Geoscience and Remote Sensing*, 40(11), 2384–2391.
- 420 Timco, G., & Weeks, W. (2010). A review of the engineering properties of sea ice.
421 *Cold regions science and technology*, 60(2), 107–129.
- 422 van den Broeke, M. (2005). Strong surface melting preceded collapse of antarctic
423 peninsula ice shelf. *Geophysical Research Letters*, 32(12).
- 424 Van der Veen, C. (1998). Fracture mechanics approach to penetration of surface
425 crevasses on glaciers. *Cold Regions Science and Technology*, 27(1), 31–47.
- 426 Wille, J. D., Favier, V., Jourdain, N. C., Kittel, C., Turton, J. V., Agosta, C., ...
427 others (2022). Intense atmospheric rivers can weaken ice shelf stability at the
428 antarctic peninsula. *Communications Earth & Environment*, 3(1), 1–14.
- 429 Wuite, J., Rott, H., Hetzenecker, M., Floricioiu, D., De Rydt, J., Gudmundsson, G.,
430 ... Kern, M. (2015). Evolution of surface velocities and ice discharge of larsen
431 b outlet glaciers from 1995 to 2013. *The Cryosphere*, 9(3), 957–969.